IAEA
INTERNATIONAL ATOMIC ENERGY AGENCY

21st IAEA Fusion Energy Conference

Chengdu, China, 16-21 October 2006

IAEA-CN-149 / EX / 8-5Rb

Theoretical Understanding of Core Transport Phenomena in ASDEX Upgrade

C. Angioni[1], R. Dux[1], A. Manini[1], A.G. Peeters[1], F. Ryter[1], R. Bilato[1], T. Dannert[1], A. Jacchia[2], F. Jenko[1], C.F. Maggi[1], R. Neu[1], T. Pütterich[1], J. Schirmer[1], J. Stober[1], W. Suttrop[1], G. Tardini[1], and the ASDEX Upgrade Team

[1]Max-Planck-Institut für Plasmaphysik, EURATOM Association, D-85748 Garching, Germany
[2]Istituto di Fisica del Plasma, Associazione Euratom–ENEA–CNR, Milano, Italy

Theoretical Understanding of Core Transport Phenomena in ASDEX Upgrade

C. Angioni[1], R. Dux[1], A. Manini[1], A.G. Peeters[1], F. Ryter[1], R. Bilato[1], T. Dannert[1], A. Jacchia[2], F. Jenko[1], C.F. Maggi[1], R. Neu[1], T. Pütterich[1], J. Schirmer[1], J. Stober[1], W. Suttrop[1], G. Tardini[1], and the ASDEX Upgrade Team

[1]Max-Planck-Institut für Plasmaphysik, EURATOM Association, D-85748 Garching, Germany
[2]Istituto di Fisica del Plasma, Associazione Euratom–ENEA–CNR, Milano, Italy
e-mail: Clemente.Angioni@ipp.mpg.de

Abstract Results obtained by comparing experimental observations of core transport phenomena in ASDEX Upgrade and predictions based on the theory of core tokamak plasma microinstabilities are presented. In contrast to neoclassical transport, it is shown that turbulent transport does not involve mechanisms of strong central impurity accumulation, in agreement with the experimental observation that central accumulation can be suppressed by increasing the auxiliary central heating. Two main properties of the trapped electron mode turbulence, namely the existence of a threshold and the stabilization produced by collisions, are demonstrated experimentally. The strong link between ion heat transport and momentum transport is quantified experimentally by power balance analysis and found in agreement with gyrokinetic calculations for the ion temperature gradient modes. Strong confinement degradation is observed in low density plasmas, when auxiliary electron heating is added to dominant ion heating. It is shown that the related ion temperature drop is consistent with the reduction of the ion temperature gradient mode threshold due to the combined effects of both the increase of the electron to ion temperature ratio and the drop of the plasma toroidal rotation.

1. Introduction

The ASDEX Upgrade tokamak is particularly well–suited for the experimental investigation of transport properties of fusion plasmas. The presence of three additional heating systems, neutral beam injection (NBI) heating, ion cyclotron (ICRH) and electron cyclotron (ECH) resonance heating, allows the exploration of a rather large range of experimental conditions. In particular, the ECH system turns out to be extremely useful for transport studies, given the unique possibility it offers to heat the electrons in a localized and externally controlled way.

The observed response of the plasma to externally induced variations of the heat fluxes provides an extremely useful experimental bed on which predictions of theoretical models can be compared. The theory of plasma micro–instabilities like ion temperature gradient (ITG) and trapped electron modes (TEM) as well as electron temperature gradient (ETG) modes is the framework within which experimental observations are compared with theoretical predictions and tentatively understood.

In this paper we report on the theoretical understanding achieved on the behaviour of different transport channels when varying the electron and/or ion heat fluxes. In particular, in the next section observations of the core behaviour of highly charged impurities in AUG is compared with predictions of the turbulent transport theory. In Section III, the electron heat transport is experimentally quantified by means of transient transport techinques and compared with quasi–linear predictions obtained for TEMs. In Section IV, the coupling between heat and momentum transport and its effects on confinement are investigated.

2. Anomalous impurity transport

Core transport governs the accumulation of highly charged impurities originating from the walls, as well as of helium ash produced in the centre of a burning plasma. Hence core impurity transport can have important consequences on the plasma performance, up to a radiative collapse. However, the effort of going beyond the neoclassical theory and provide a theoretical description of the experimental observations also when they exceed the neoclassical predictions started only very recently. The experimental study of impurity transport in AUG is receiving

more and more importance since an increasing amount of plasma facing components is covered by tungsten–armour.

Over an extended dataset of H–mode discharges, it is observed that the brightness of the central bolometer line of sight is proportional to the brightness of a peripheral line of sight (tangent at $\rho \simeq 0.4$) in all plasmas which have central wave heating, ICRH or ECH, or are sawtoothing, while plasmas without sawteeth and without central wave heating show a central brightness which is much larger [1]. These large differences can only be explained by strong central radiation of medium-Z to high-Z elements, which must have large density gradients inside $\rho \simeq 0.4$. These results motivated a set of dedicated experiments with Si laser ablation to quantify the effects [2]. The Si central diffusivity is strongly increased from neoclassical values up to almost one order of magnitude larger than neoclassical, when central wave heating is added. Correspondingly it is observed that the central effective heat conductivity increases by an order of magnitude, being at neoclassical levels before the switch–on of wave heating, and becoming strongly anomalous afterwards.

From these observations, the use of central wave heating as a control tool to avoid tungsten accumulation has become regular on AUG, where the use of ECH is more efficient [1,3,4]. Figure 1 shows an example of the strong effect of central ECH on the W behaviour [1].

As revealed by the Si trace experiments [2], central wave heating not only can have the effect of reducing the central main ion density peaking, and therefore the neoclassical inward drift, but also of increasing the central diffusion above neoclassical levels. Moreover, the reduction of density peaking would not be sufficient to explain the suppresion of impurity accumulation within neoclassical theory alone, as shown by specific neoclassical calculations [5] with the NEOART code [6,7].

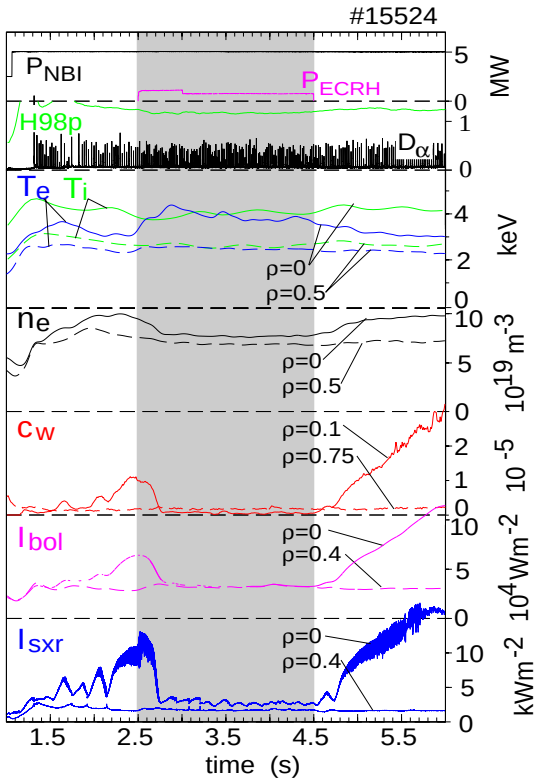

Figure 1: Time traces of the AUG H–mode discharge ♯15524. Plotted parameters are quoted in the figure.

Therefore the general result in AUG is that when central heat transport is anomalous, high Z impurities are not observed to accumulate. It must be emphasized that we refer to the very central region of the plasma, where the temperature gradients flatten, unless a strongly localized heat source is provided. This very general experimental result implies that, to be in agreement with the experimental observations, turbulent transport theory should not predict any mechanism of impurity accumulation which diverges with increasing Z, for AUG plasma parameters. This is in contrast to neoclassical theory, within which a mechanism for impurity accumulation diverging with increasing Z is predicted.

In order to verify this experimental result within the theory of ion temperature gradient (ITG) and trapped electron mode (TEM) microinstabilities, we have used the linear version of the gyrokinetic code GS2 [8] and made quasi-linear estimates of the particle flux of a trace impurity by means of a quasi–linear model which has been fixed by comparisons with the non–linear results of the GENE code [9,10].

In a mainly electrostatic turbulent plasma, three main mechanisms transporting impurities can be indentified in a simple fluid model, and their relative magnitude has been recently computed with a gyrokinetic code [11]. The first is the $E \times B$ advection and compression. The advection contributes to the diagonal transport, while the compression provides a charge

independent inward pinch often called curvature or q–pinch [12,13], and which corresponds to the same pinch mechanism identified by the Turbulent Equipartition theory [14,15]. The second mechanism, usually called thermodiffusion, comes from the coupling with temperature fluctuations via the ∇B and curvature drift and causes a pinch term which is proportional to the logarithmic impurity temperature gradient, and decreases with the impurity charge as a consequence of the inverse charge dependence of the curvature drift [16,17,11]. The third mechanism, which we have recently pointed out for the first time, is linked to parallel compression of parallel velocity fluctuations produced along the field line by the fluctuating electrostatic potential [11]. This pinch term is proportional to the ratio of the charge to the mass number of the impurity, and therefore does not vanish for sufficiently ionized heavy impurities. The peculiarity of the last two pinch mechanisms is that their direction changes sign as a function of the direction of propagation of the instability. For instabilities rotating in the electron (ion) diamagnetic direction, the thermodiffusion term is directed inward (outward), while the parallel compression pinch is directed outward (inward). The total turbulent pinch results as a complex combination of at least these three mechanisms and therefore is connected with the dominant instabilities in the plasma and finally with its turbulente state. However, what is important to observe is that none of these particle pinch terms involves a mechanism of diverging impuritiy peaking as a function of Z.

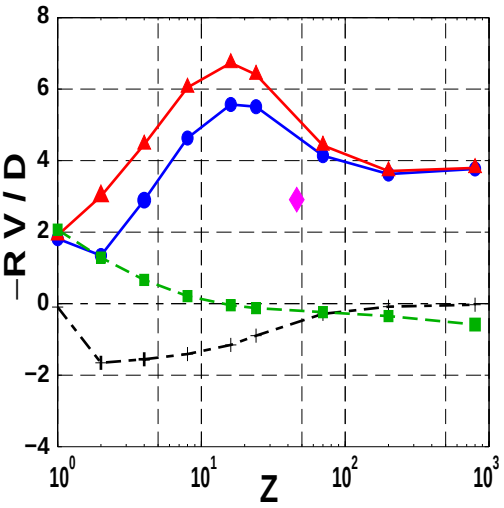

Figure 2: Normalized pinch to diffusion ratio as computed by a quasi–linear model with the GS2 code, as a function of Z, with $A = 2Z$ for different choices of input parameters related to the experimental profiles of the ECH phase of the AUG shot ♯15524 as explained in the text.

Figure 2 shows the Z dependence of the pinch to diffusion ratio $-RV/D$ for a trace impurity as computed with GS2 for average plasma parameters of the AUG H–mode plasma presented in Figure 1 during the ECH phase, taken in the radial interval $0.35 \leq$ r/a ≤ 0.55. The mass of the impurity has been taken equal to $A = 2Z$ in the Z scan. Calculations of trace impurity transport are performed by including a third species in negligible charge concentration ($n_Z Z/n_e \leq 1/1000$) in the input parameters. Since for a trace impurity the particle flux is linear in the logarithmic density gradient, this allows us to determine unambiguously, by linear fit of the code results, a diffusion coefficient and a pinch velocity [11]. We note that the dimensionless ratio $-RV/D$ is independent of the factor estimating the saturation amplitude of the electrostatic potential fluctuations in the quasi–linear model and is equal to the dimensionless logarithmic gradient of the density profile R/L_n of the trace impurity in steady–state conditions, when neoclassical and source contributions are negligible.

In Figure 2, circles show the dependence obtained when the actual plasma parameters are used, namely $\varepsilon = 0.16$, $q = 1.4$, $s = 0.8$, $R/L_{Te} = 6.5$, $R/L_{Ti} = 5.0$, $R/L_n = 2.0$, $T_e = T_i$, where the impurity temperature profile has been taken equal to the deuterium temperature. The dominant instability is found to be an ITG, despite $R/L_{Te} > R/L_{Ti}$, due to the relatively high collisionality and the rather small density gradient of this plasma. The curve with triangles shows the results of similar calculations but considering a flat temperature gradient for the trace impurity. This allows us to single out the contribution due to thermodiffusion (curve with crosses in the figure), which is found to be directed outwards, as the negative sign indicates, consistently with the ion diamagnetic direction of rotation of these modes. Moreover the curve with squares shows the results obtained in the case that a dominant TEM instability is present, which has been obtained by increasing the logarithmic electron temperature gradient up to 9,

and decreasing the collisionality by a factor 5. In this case the thermodiffusion contribution (not shown) is directed inwards, and for large values of Z, where thermodiffusion becomes small, the outward parallel compression pinch balances the inward $E \times B$ compression pinch to provide a total pinch very close to zero and a flat or even slightly hollow density profile for highly charged impurities. The effect of the parallel compression pinch is also visible in the case W is considered in an experimentally observed ionisation stage, namely W^{46+}. For the experimental input parameters, this is shown in the figure by the diamond point ($Z = 46$ and $A = 184$). The reduction of the pinch to diffusion ratio with respect to the curve $A = 2Z$ is due exclusively to a reduction of the inward pinch and is attributed to the reduction of the parallel compression pinch, which is directed inwards for ITG instabilities. The diffusion coefficient is instead the same as the one obtained in the case $A = 2Z$, showing that the diffusion coefficient becomes independent of A at large values of A [11]. The pinch is caused by the reduction of the Z/A ratio to which the parallel compression pinch is proportional [11]. The calculation for W^{46+} delivers a logarithmic density gradient $R/L_{nW} = 2.9$, not too far from the corresponding value for electrons, consistent with a rather flat concentration profile, as observed in the experiments during the ECH phase. More in general, the reduction of the pinch to diffusion ratio of highly charged trace impurities predicted in the case of dominant TEM instabilities is in qualitative agreement with the observation of an efficient flattening of the impurity density profiles in the presence of auxiliary electron heating observed in tokamaks [2,18,19]. The overall result that turbulent transport does not predict mechanisms of impurity pinch which diverge with increasing Z is in agreement with the whole set of experimental observations in AUG. It is also promising for a burning plasma, provided the central α heating be large enough to drive a turbulent transport up to the innermost region of the plasma column.

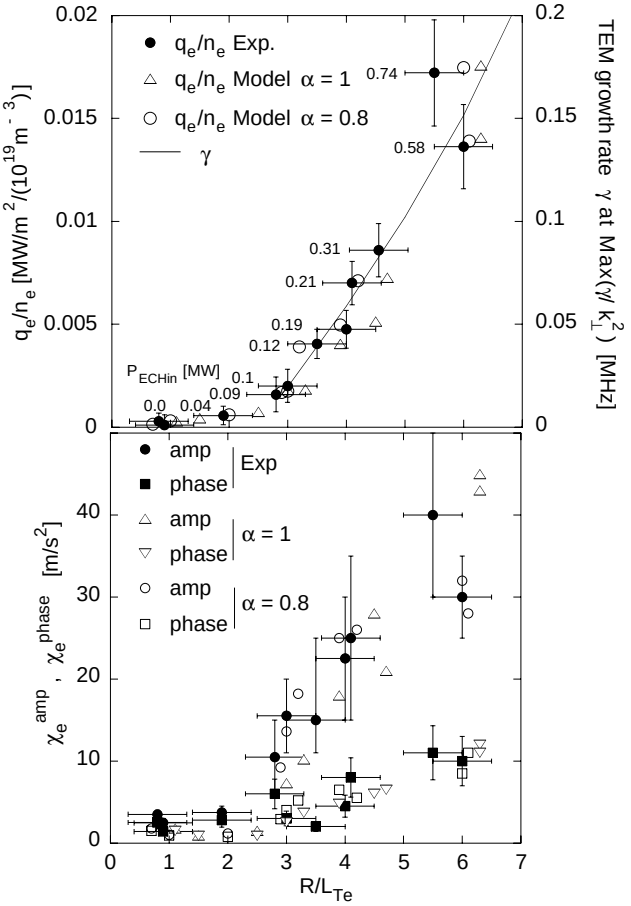

Figure 3: Upper plot: electron heat flux versus R/L_{Te}, experimental data, empirical and theoretical models. Lower plot: χ_e^{amp} and χ_e^{phase} versus R/L_{Te}, experimental and modelling data.

3. Experimental identification of trapped electron mode turbulence properties

In AUG experiments to vary the normalized logarithmic electron temperature gradient R/L_{Te} were carried out using a combination of on–axis and off–axis ECH [20], while keeping the total electron heating power constant. The results pointed towards a finite value of R/L_{Te} as the electron heat flux tends to zero. A comparison of these results with linear calculations obtained with the GS2 code found that dominant instabilities in these experimental conditions are the TEMs and showed a good agreement of the heat flux dependence upon R/L_{Te} [21]. Analogous conclusions are drawn in similar recent experiments carried out in DIII–D [22] and TCV [23]. However in none of these experiments an explicit evidence of the existence of the threshold is provided, since the experimental conditions were never such to allow the electron temperature to be below the threshold. More recently, experiments in AUG have been performed

in such conditions that an explicit demonstration of the existence of a threshold is provided, since clear signatures of a transition from below to above the threshold are observed [24]. The most complete investigations of transport are obtained when analyses from power balance and transient phenomena are carried out simultaneously, and to this purpose the power modulation of localized ECH is extremely well suited.

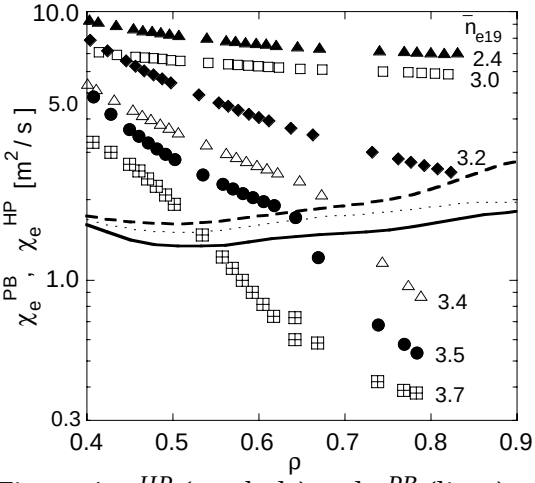

Figure 4: χ_e^{HP} (symbols) and χ_e^{PB} (lines) as a function of the normalized minor radius for different values of the line average density.

Similarly to previous experiments [20], the ECH is deposited both on-axis and off-axis keeping constant the total heat power, 0.65 MW in the new experiments, but differently from previous experiments, in the new experiments [24] the plasma current has been reduced from 800 kA to 400 kA, reducing the Ohmic heating power and therefore reducing the heat flux in the centre to much smaller values than in previous experiments in conditions of dominant off-axis ECH. The experimental results are presented in Fig. 3, together with modelling results obtained with an empirical model [25] and with the gyrokinetic code GS2. The experimental heat flux exhibits a clear change of slope at R/L_{Te} = 3. The levels of central ECH power are quoted in the figure to show the fine heat flux scan required at low values of R/L_{Te}. The simulations with the empirical transport model $\chi_e = q^{1.5}\,(T_e/eB)(\rho_s/R)[\chi_s(R/L_{Te} - R/L_{T_{cr}})^{\alpha}\,H(R/L_{Te} - R/L_{T_{cr}}) + \chi_0]$,[25], with two choices of the exponent α, show a good agreement with the data. The same agreement is found with the results of linear GS2 [8] calculations which use experimental values as input parameters, and yield the growth rate at the maximum value in the k_θ spectrum of the ratio of the growth rate to the square of the perpendicular wave vector, $\gamma/k_\perp^2$. This linear quantity is shown to describe rather accurately the behaviour of the electron heat flux in non–linear calculations of the TEM turbulence [9]. The jumplike increase observed in both χ_e^{amp} and χ_e^{phase} around R/L_{Te} is an additional and consistent evidence of the transition through a threshold, in this case obtained by transient transport analyses. The fact, that, differently from what it is usually to be expected, $\chi_e^{amp} > \chi_e^{phase}$, provides a further indication of the existence of the threshold, as demonstrated by the consistent behaviour of the results of the empirical model and as explained in detail in [24].

Another property of TEMs is the stabilization with increasing collisionality (e.g. [10]). This theoretically predicted property has been investigated experimentally in discharges at 600 kA in which the line averaged density has been increased in a linear ramp from 2.2 10^{19} m^{-3} to 3.7 10^{19} m^{-3}. In Fig. 4, a strong decrease of χ_e^{HP} is observed with increasing density, and therefore collisionality since the heating power is constant. In particular, at the highest density values, χ_e^{HP} is found to drop below χ_e^{PB}. This indicates the rather unusual situation in which the electron heat flux remains large but rather independent of the electron temperature gradient. Micro–stability analyses with GS2 of these plasmas indicate that at low density the dominant instability is the TEM, while it becomes the ITG for the highest density values, due to the combined effect of the increase of collisionality and the decrease of T_e/T_i (see Figs. 3 and 4 in [24]). While in these experimental conditions an increase of R/L_{Te} implies an increase of the electron heat flux for the TEM, for the ITG it is found that the electron heat flux is almost independent of R/L_{Te}. Hence, the experimental results presented in Fig. 4 can be explained by a transition from dominant TEM to dominant ITG instability in this plasmas with increasing density. Consistent behaviours connected to a transition from TEM to ITG with increasing collisionality are observed in similar experimental conditions on the particle transport behaviour [26] and reflectometry measurements of the perpendicular rotation velocity of density fluctuations [27].

4. Correlations between momentum and heat transport

In AUG a strong link between toroidal momentum transport and ion heat transport is observed [28]. This is consistent with previous observations in DIII–D [29] and more recently in JET [30]. Figure 5 shows the co–linearity observed between ion temperature and toroidal velocity gradients over a dataset of plasmas heated with all the different auxiliary heating systems available in AUG. Assuming the following diffusive laws for both the ion temperature and the toroidal velocity,

$$Q_i = n_i \chi_i \nabla T_i \quad \text{and} \quad \Gamma_\phi = m n_i \chi_\phi \nabla v_\phi,$$

a general relationship holds between temperature and velocity gradients which can be expressed in the form

$$\nabla T_i \left(1 + \frac{Q_{i,ICH}}{Q_{i,NBI}}\right)^{-1} = \frac{\chi_\phi}{\chi_i} \frac{m Q_{i,NBI}}{\Gamma_\phi} \nabla v_\phi$$

where it has been assumed that equipartition is small in these plasmas and can be neglected with respect to direct NBI and ICRH ion heating, namely $Q_i \simeq Q_{i,NBI} + Q_{i,ICH}$ (note that ECH does not provide direct ion heating). Hence, the co–linearity observed in Fig. 5 shows that a connection exists between ion heat and momentum transport which can be described as a proportionality between the ion heat and the momentum conductivities. These have been computed by power balance analysis with the ASTRA code. The beam heating powers and collisional torque densities have been computed by the Monte Carlo FAFNER code for all the observations of the dataset, the trapped beam ions torque by a parametrization over a set of TRANSP runs, and the ICRH power densities profiles by a set of TORIC runs [31]. A strong correlation between χ_ϕ and χ_i is observed, as shown in Figure 6, in which the probability distribution of observations of the ratio $\chi_\phi/(\chi_i - \chi_{i,neo})$ is plotted for three different radial positions. At $r/a = 0.5$ the majority of observations have a ratio $\chi_\phi/(\chi_i - \chi_{i,neo})$ between 0.9 and 1.3 ($\chi_\phi/\chi_i \approx 1.0$) while at $r/a = 0.7$ most of the observations have a ratio around 0.75 ($\chi_\phi/\chi_i \approx 0.65$). The reduction of this ratio as a function of the minor radius was already reported in [28], but is found weaker in the present study. This depedence is also consitent with local estimates of the ratio of the momentum to ion energy replacement times in DIII–D [29]. These experimentally determined values are in promising agreement with recent theoretical estimates obtained by linear gyrokinetic calculations for ITG instabilities [32], which identify a ratio $\chi_\phi/\chi_{i,turb} \simeq 0.8$, rather independent of several plasma parameters. The physical mechanism behind the observed dependence on minor radius has not been identified yet. Trapped particle effects, which were not included in the calculations in [32], might be the cause. The proportionality between ion heat and momentum conductivity does not involve causality. It just indicates that ITG turbulence is equally efficient in transporting both ion energy and toroidal momentum.

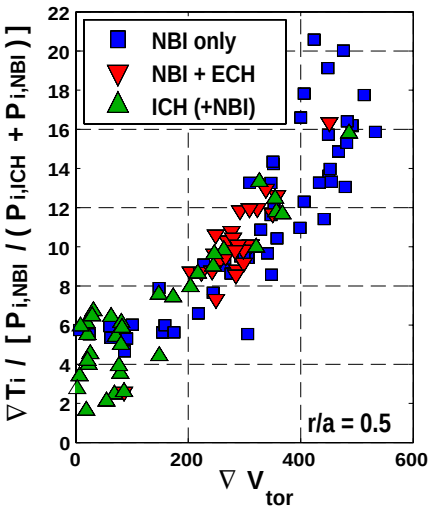

Figure 5: Relationship between the ion temperature gradient (in keV/m) normalized to the fraction of beam heating power and the toroidal velocity gradient in [km/s /m] for a dataset of AUG discharges with NBI, ECH and ICRH heating.

This relationship does not exclude that rotation by itself can have effects on transport of both heat and momentum. While the ratio of χ_ϕ/χ_i remains constant, a reduction of the toroidal velocity, triggered by an increase of transport or an externally imposed reduction of the torque, may imply a variation of both χ_ϕ and χ_i.

From the theoretical standpoint, microinstabilities are affected by the presence of a radial gradient of the toroidal velocity by two opposite mechanisms. The parallel velocity shear has

a destabilizing effect and can also drive a microinstability itself, above a certain threshold (e.g. [32]). On the other hand a radial gradient of the toroidal velocity contributes to the $E \times B$ velocity, which controls the level of transport through shear flow stabilisation.

We observe a positive correlation in the data between R/L_{Ti} and $R\nabla V_\phi/v_{thi}$, which indicates that the stabilization by means of the ω_{ExB} shearing rate dominates over the destabilization due to the parallel velocity shear [32]. The experimentally measured values of R/L_{Ti} fall in the theoretically predicted range of values of the ITG threshold. A detailed comparison between the experimentally measured values of R/L_{Ti} and the linear ITG threshold has been performed for a subset of low density (below 5 10^{19} m^{-3}) plasmas with identical global parameters in which phases with 5 MW NBI heating only are followed by phases in which up to 2 MW of ECH are added [33]. The ITG threshold is determined as the value of R/L_{Ti} at which the linear growth rate of the mode γ_{GS2} computed by GS2 [8] equals the value of ω_{ExB} [34]. As shown in Figure 7, a good agreement between the experimentally measured values of R/L_{Ti} and the ITG threshold at mid–radius is found, provided that both destabilizing effects of the increase of the T_e/T_i ratio and the reduction of the toroidal rotation gradient are taken into account [35]. Such a drop of the ion temperature profile in response to the switch–on of ECH is connected with a strong reduction of the confinement time, which is measured to decrease from 0.12 s to 0.08 s when the auxiliary heating power is increased from 5 MW of NBI to 5 MW of NBI and 2 MW of ECH. Hence in these conditions, the observed confinement degradation, likely caused by the drop of the ITG threshold due to the combined effects of an increase T_e/T_i and a reduction of plasma rotation as presented above, exceeds the usual scalings of confinement time degradation with increasing power.

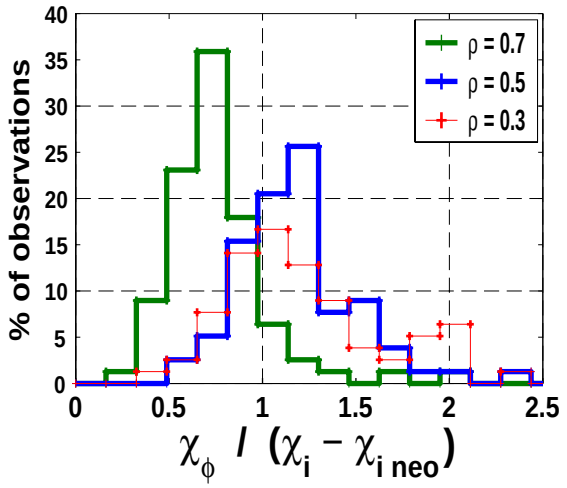

Figure 6: Distribution of $\chi_\phi/(\chi_i - \chi_{i,neo})$ over a database of 80 observations at three different radial positions

5. Summary and conclusions

Advances in the theoretical understanding of core transport phenomena in AUG have been presented.

It has been shown that, differently from neoclassical theory, no mechanism of strong impurity accumulation is predicted by the theory of core microinstabilities, in agreement with the regular observation in AUG that central impurity accumulation can be suppressed by an increase of the heat flux at the centre of the plasma column, driving the transport anomalous up to the very centre.

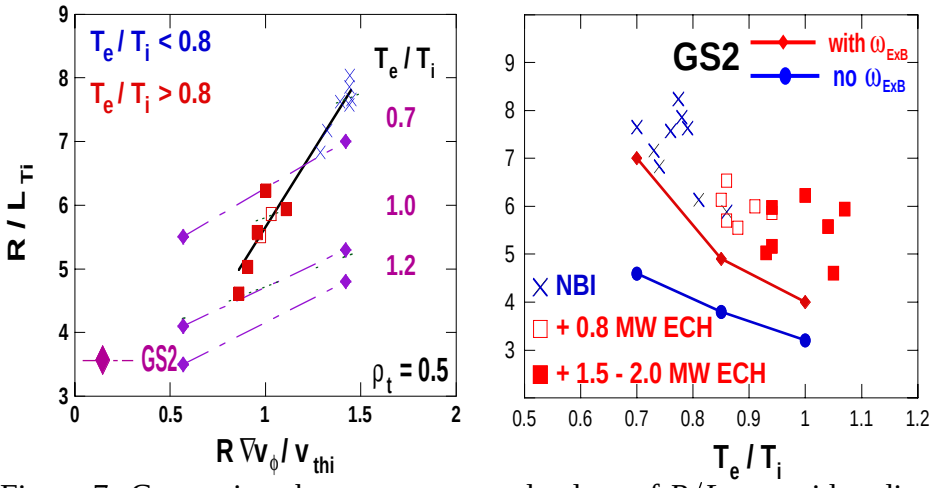

Figure 7: Comparison between measured values of R/L_{Ti} at mid–radius and the ITG threshold dependences on $R\nabla v_\phi/v_{thi}$ (by means of the ω_{ExB} stabilisation) and T_e/T_i.

The main properties of the trapped electron mode instabilities, namely the existence of a threshold and the stabilization with increasing collisionality, have been demonstrated experimentally, sheding new light on the mechanisms producing electron heat transport in the plasma core.

A strong correlation between ion heat and momentum transport in AUG has been documented and the ratio between the experimentally determined ion heat conductivity and the momentum conductivity is found to be close to the predictions obtained by linear gyrokinetic calculations of ITG microinstabilities. Finally, the reduction of the normalized logarithmic ion temperature gradient observed in response to electron cyclotron heating in plasmas heated by neutral beam heating is found in agreement with the predicted variation of the ion temperature gradient mode threshold, provided that both the destabilizing effects of the increase of the electron to ion temperature ratio and the reduction of the toroidal velocity gradient are taken into account.

Acknowledgments

The Authors thank W. Dorland and M. Kotschenreuther for providing the gyrokinetic code GS2, and D. McCune for providing the code TRANSP.

References

[1] Neu R *et al* 2003 *J. Nucl. Mater.* **313–316** 116.
[2] Dux R *et al* 2003 *Plasma Phys. Control. Fusion* **45** 1815.
[3] Dux R 2003 *Fusion Tech.* **44** (2003) 708.
[4] Neu R *et al* 2005 *Nucl. Fusion* **45** 209.
[5] Dux R 2004 Impurity transport in tokamak plasmas *Report IPP 10/27* Garching.
[6] Peeters AG 2000 *Phys. Plasmas* **7** 268.
[7] Dux R, Peeters AG 2000 *Nucl. Fusion* **40** 1721.
[8] Kotschenreuther M *et al* 1995 *Comput. Phys. Commun.* **88** 128.
[9] Dannert T, Jenko F 2005 *Phys. Plasmas* **12** 072309.
[10] Angioni C *et al* 2005 *Phys. Plasmas* **12** 112310.
[11] Angioni C and Peeters AG 2006 *Phys. Rev. Lett.* **96** 095003.
[12] Weiland J *et al* 1989 *Nucl. Fusion* **29** 1810.
[13] Garbet X *et al* 2003 *Phys. Rev. Lett.* **91** 035001.
[14] Isichenko MB *et al* 1996 *Phys. Rev. Lett.* **74** 4436.
[15] Baker DR and Rosenbluth M 1998 *Phys. Plasmas* **5** 2936.
[16] Frojdh M *et al* 1992 *Nucl. Fusion* **32** 419.
[17] Garbet X *et al* 2005 *Phys. Plasmas* **12** 082511.
[18] Scavino E *et al* 2004 *Plasma Phys. Control. Fusion* **46** 857.
[19] Puiatti ME *et al* 2006 *Phys. Plasmas* **13** 042501.
[20] Ryter F *et al* 2003 *Nucl. Fusion* **43** 1396.
[21] Peeters AG *et al* 2005 *Phys. Plasmas* **12** 022505.
[22] Deboo JC *et al* 2005 *Nucl. Fusion* **45** 494.
[23] Camenen Y *et al* 2005 *Plasma Phys. Control. Fusion* **47** 1971.
[24] Ryter F *et al* 2005 *Phys. Rev. Lett.* **95** 085001.
[25] Garbet X *et al* 2004 *Plasma Phys, Controlled Fusion* **46** 1351.
[26] Angioni C *et al* 2005 *Phys. Plasmas* **12** 040701.
[27] Conway GD *et al* 2006 *Nucl. Fusion* **46** S799.
[28] Nishijima D *et al* 2003 *Plasma Phys. Controlled Fusion* **47** 89.
[29] deGrassie JS *et al* 2003 *Nucl. Fusion* **43** 142.
[30] de Vries P *et al* 2006 *Plasma Phys. Controlled Fusion* to be submitted.
[31] Brambilla M and Bilato R, 2006 *Nucl. Fusion* **46** S387.
[32] Peeters AG *et al* 2005 *Phys. Plasmas* **12** 072515.
[33] Manini A *et al* 2004 *Plasma Phys, Controlled Fusion* **46** 1723.
[34] Waltz RE *et al* 1994 *Phys. Plasmas* **1** 2229.
[35] Manini A *et al* 2006 *Nucl. Fusion* submitted.